Nanosphere Lithography: Tunable Localized Surface Plasmon Resonance Spectra of Silver Nanoparticles

Traci R. Jensen,† Michelle Duval Malinsky, Christy L. Haynes, and Richard P. Van Duyne*

Department of Chemistry, Northwestern University, Evanston, Illinois 60208-3113

Received: July 6, 2000; In Final Form: September 8, 2000

The wavelength corresponding to the extinction maximum, λ_{max}, of the localized surface plasmon resonance (LSPR) of silver nanoparticle arrays fabricated by nanosphere lithography (NSL) can be systematically tuned from ∼400 nm to 6000 nm. Such spectral manipulation was achieved by using (1) precise lithographic control of nanoparticle size, height, and shape, and (2) dielectric encapsulation of the nanoparticles in SiO_x. These results demonstrate an unprecedented level of wavelength agility in nanoparticle optical response throughout the visible, near-infrared, and mid-infrared regions of the electromagnetic spectrum. It will also be shown that this level of wavelength tunability is accompanied with the preservation of narrow LSPR bandwidths (fwhm), Γ. Additionally, two other surprising LSPR optical properties were discovered: (1) the extinction maximum shifts by 2−6 nm per 1 nm variation in nanoparticle width or height, and (2) the LSPR oscillator strength is equivalent to that of atomic silver in gas or liquid phases. Furthermore, it will be shown that encapsulation of the nanoparticles in thin films of SiO_x causes the LSPR λ_{max} to red shift by 4 nm per nm of SiO_x film thickness. The size, shape, and dielectric-dependent nanoparticle optical properties reported here are likely to have significant impact in several applications including but not limited to the following: surface-enhanced spectroscopy, single-molecule spectroscopy, near-field optical microscopy, nanoscopic object manipulation, chemical/biological sensing, information processing, data storage, and energy transport in integrated optical devices.

I. Introduction

The signature optical property of noble metal nanoparticles is the localized surface plasmon resonance, hereafter LSPR. When metal nanoparticles are excited by electromagnetic radiation, they exhibit collective oscillations of their conduction electrons known as localized surface plasmons. The wavelength corresponding to the extinction maximum, λ_{max}, of the LSPR is highly dependent on the size, shape, and dielectric properties of the metal nanoparticles.[1] The primary consequences of LSPR excitation are selective photon absorption, scattering, and local electromagnetic field enhancement. The ability to manipulate and predict the LSPR of metal nanoparticle systems is desirable in several technological applications. For example, it has recently been demonstrated both theoretically[2] and experimentally[3] that the coupling of surface plasmons in linear chains of metal nanoparticles results in the transport of light along the direction of the chain. Also, the excitation of surface plasmons in illuminated metallic near-field scanning optical microscopy (NSOM) probes is responsible for the large enhancements in the electric fields originating from the sharply pointed tip.[4] Similarly, the operation of scanning tunneling[5] and scanning force[6,7] microscopes used in FOLANT configuration also uses surface plasmon excitation to focus laser radiation in the near field of the tip where it is used to nanostructure materials by local heating. Ebbesen et al.[8] have also reported that the coupling of incident light with surface plasmons in a 200 nm thick Ag film with 150 nm cylindrical holes resulted in a 100-fold increase in the intensity of transmitted light. The findings listed above are just a few examples of how control of the LSPR in nanoengineered materials can be used to transport optical energy or to focus large concentrations of light into small volumes.[9] The ability to manipulate electromagnetic radiation in such a manner will be useful in various types of NSOMs[10−13] and integrated optical circuits. Other examples of applications that will benefit from the understanding and control of the LSPR include but are not limited to the following: nanoparticle manipulation by optical trapping[14,15] and optical tweezers,[4] ultrafast optical switching,[16−18] optical bistability,[19,20] chemical and biological sensing,[21,22] optical filters,[23,24] surface-enhanced Raman spectroscopy (SERS),[25−36] and other surface-enhanced spectroscopies.[37−41]

Within this broad spectrum of applications, the LSPR of metal nanoparticle systems, particularly those of Ag and Au, is probably best known as the source of the local electromagnetic field enhancement thought to be the dominant contribution to the large intensities observed in SERS. Although thousands of studies have appeared in the literature since the discovery of SERS,[42] a comprehensive understanding of the enhancement mechanism(s) responsible for the 10^6 enhancement factor still remains elusive. This unsatisfactory situation has recently been greatly exacerbated by the extraordinary finding that SERS can be observed with an enhancement factor of 10^{14}−10^{15}.[26,34] Enhancement factors at this level permit the observation of signals from single molecules, both resonant and nonresonant with the laser excitation wavelength, adsorbed on colloidal Ag nanoparticles.[26−34,43] Emory and Nie specifically demonstrated that Ag colloidal nanoparticles of distinct sizes and shapes display enormous enhancement factors on the order of 10^{14}−10^{15}.[26,27] These "hot particles" have a very narrow size range

* Author to whom correspondence should be addressed. E-mail: vanduyne@chem.nwu.edu.

† Present address: Omega Optical, Inc., Brattleboro, VT.

10.1021/jp002435e CCC: $19.00
Published on Web 10/21/2000

where the enhancement properties are optimized for a given laser excitation wavelength.[29] Their results strongly support the idea that size-dependent LSPRs contribute to SER signals intense enough to detect single molecules. Making the situation even more complicated, the single-molecule SERS experiments of Kneipp and co-workers[32−34] suggest that the ultra-intense Raman signals occur only from aggregates of Ag nanoparticles and that the detected molecules are adsorbed between nanoparticles. Thus, it is currently open to debate whether single-molecule SERS is a single or multiple nanoparticle phenomenon. The ability to understand in detail how the LSPR of individual nanoparticles and their arrays depend on size, shape, interparticle coupling, and external dielectric environment will be likely to play a key role in unraveling the mechanism of single-molecule SERS.

To systematically examine the LSPR of nanoparticle systems, a fabrication method that produces nanoparticles with homogeneous sizes and shapes is required. Nanolithographic methods provide an ideal way of preparing arrays of particles on a substrate with controlled size, shape, and spacing. Several optical extinction studies have been reported where electron beam lithography was used to prepare the nanoparticle array.[44−47] In other optical investigations, rod-shaped nanoparticles with variable aspect ratios have been produced using a variety of procedures.[48−51] Additionally, Halas and co-workers[52−54] have cleverly fabricated Au nanoshell materials by chemical reduction of Au (III) onto silica nanosphere cores. The optical extinction spectra of these core−shell nanoparticles exhibit a LSPR that is wavelength tunable from 550 nm in the visible to 2000 nm in the near-infrared.[52,53] Wavelength tunability was achieved by varying the relative dimensions of the core and shell. Although this approach allows significant control over the value of λ_{max}, the LSPR bandwidths (fwhm), Γ, observed in these experiments were broad enough that the quality factor, $Q = \lambda_{max}/\Gamma$, had estimated values of 2 for visible resonances[53] and ≤ 1 for near-infrared resonances.[52]

In the study reported here, we used nanosphere lithography (NSL) to fabricate size-tunable Ag nanoparticles.[55,56] NSL provides outstanding control of nanoparticle size, shape, and interparticle spacing. The in-plane width, *a*, and out-of-plane height, *b*, of NSL-fabricated nanoparticles can be independently tuned with nanometer precision by selection of the nanosphere diameter, *D*, used in the 2D colloidal crystal deposition mask and the mass thickness of the material deposited, d_m. Nanoparticle shape is controlled by the precision of the 2D colloidal crystal mask or alternatively by postdeposition processing steps such as thermal annealing. Additionally, NSL is extremely simple to implement, low cost, and quite materials general, making it nearly ideal as a platform for theory vs experiment studies of nanoparticle optical properties. In a very real sense, the experiments reported here are the experimental equivalent of the theoretical size-dependent LSPR studies published 13 years ago by Zeman and Schatz.[57]

The purpose of this paper is to demonstrate that the LSPR extinction maximum of a single nanoparticle material system, Ag, can be continuously tuned throughout the visible, near-infrared, and mid-infrared regions of the electromagnetic spectrum. This will be achieved through independent manipulation of nanoparticle size, shape, and external dielectric environment. Furthermore, we will discuss five additional new features associated with the nanoparticle optics of Ag that were not previously known: (1) λ_{max} is extremely sensitive to nanoparticle structure with sensitivity factors, $\Delta\lambda_{max}/\Delta a$ and $\lambda_{max}/\Delta b$, in the range of 2 to 7; (2) the thermally induced nanoparticle structural transition from triangular, T, to ellipsoidal, E, in-plane shape results in a large shift in λ_{max} by ~200 nm; (3) Ag nanoparticles can be fabricated with LSPRs characterized by $Q > 1$ over the entire range 400 nm $< \lambda_{max} <$ 6000 nm and with $Q \sim 5.4-7.6$ throughout the visible; (4) SiO_x-encapsulated Ag nanoparticles exhibit a red shift with a sensitivity factor, $\Delta\lambda_{max}/\Delta d_{SiOx}$, of 4; and (5) the oscillator strength of the Ag nanoparticle LSPR is 0.3 which is comparable to that of atomic Ag in the gas and liquid phase.

Experimental Section

Materials. Ag (99.99%, 0.50 mm diameter) was purchased from D. F. Goldsmith (Evanston, IL). Ruby red muscovite mica substrates were obtained from Asheville-Schoonmaker Mica Co. (Newport News, VA). Borosilicate glass substrates were Fisherbrand No. 2 cover slips from Fisher Scientific. Silicon(II) oxide (SiO_x) was purchased from Alpha-Aesar (Ward Hill, MA), and tungsten vapor deposition boats were acquired from R. D. Mathis (Long Beach, CA). Polystyrene nanospheres of various diameters were purchased from Interfacial Dynamics Corporation (Portland, OR). Triton X-100 was obtained from Aldrich (Milwaukee, WI). For all steps of substrate preparation, water purified with cartridges from Millipore (Marlborough, MA) to a resistivity of 18 MΩ was used.

Substrate Preparation. Glass substrates were cleaned by immersion in piranha solution (3:1 concentrated H_2SO_4:30% H_2O_2) at 80 °C for 1 h. After cooling, the substrates were rinsed repeatedly with millipure water and then sonicated for 60 min in 5:1:1 H_2O:NH_4OH:30%H_2O_2 solution. Following sonication, the substrates were again rinsed repeatedly with water and then used immediately or stored in water for no longer than one week. Mica substrates of approximately 1 cm^2 in area and 50 mm thickness were either used as received or freshly cleaved immediately before nanosphere mask formation.

Periodic Particle Array Preparation. Single-layer periodic particle arrays were prepared using the technique of nanosphere lithography.[55,56] Simply, a suspension of nanospheres was drop-coated onto the substrate where they self-assembled into a hexagonally closed-packed 2D colloidal crystal that served as a deposition mask. For nanoparticle arrays fabricated on mica substrates, the nanospheres were received as a suspension in water and were then further diluted in a 1:1 ratio with a solution of the surfactant Triton X-100 and methanol (1:400 by volume). Addition of the surfactant solution allowed for better packing over large areas of the mica substrate. Nanospheres used to form deposition masks on glass substrates were used as received without any further dilution with a surfactant solution. Once the 2D colloidal crystal deposition mask was formed, the substrates were mounted into the chamber of a Consolidated Vacuum Corporation vapor deposition system. Ag films of various thicknesses were then deposited over the nanosphere mask. The mass thickness, d_m, for each film was measured using a Leybold Inficon XTM/2 deposition monitor quartz crystal microbalance (East Syracuse, NY). After the Ag deposition, the nanosphere mask was removed by sonicating the entire substrate in either CH_2Cl_2 or absolute ethanol for 2 min. An array of triangularly shaped particles with P_{6mm} symmetry remains on the substrate. Samples subjected to a postdeposition annealing procedure were heated under vacuum at 300 °C for 1 h. Overlayers of SiO_x were grown in the same vacuum deposition system that was used to produce the Ag films.

Atomic Force Microscopy (AFM) Measurements. AFM images were collected under ambient conditions using a Digital Instruments Nanoscope III microscope operating in either

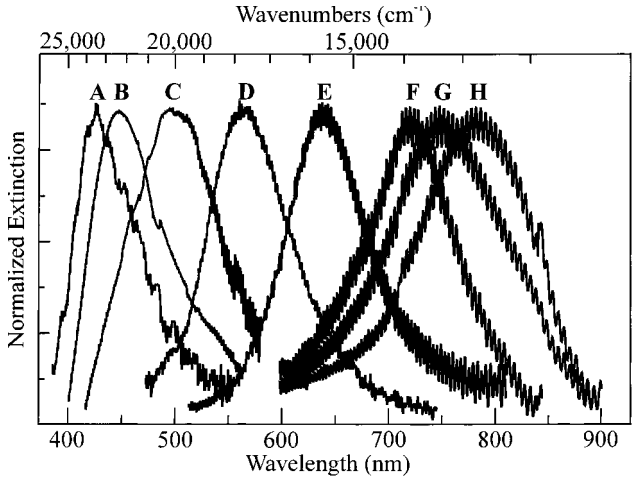

Figure 1. UV−vis extinction spectra of Ag nanoparticle arrays on mica substrates. Reported spectra are raw, unfiltered data. The oscillatory signal superimposed on the LSPR spectrum seen in the data is due to interference of the probe beam between the front and back faces of the mica. See Table 1 for nanoparticle structural parameters.

contact mode or tapping mode. Etched Si nanoprobe tips (Digital Instruments, Santa Barbara, CA) with spring constants of approximately 0.15 N m^{-1} were used. These conical shaped tips had a cone angle of 20° and an effective radius of curvature of 10 nm. The resonance frequency of the tapping mode cantilevers was measured to be between 280 and 330 kHz. The AFM images presented here represent raw, unfiltered data.

Ultraviolet−Visible Extinction Spectroscopy. Extinction spectra were recorded in standard transmission geometry using either a Beckman DU-7, Ocean Optics SD2000, or an OLIS modified Cary 14 spectrophotometer. Regardless of the instrument used, all macroextinction measurements were recorded using unpolarized light with a probe beam size of approximately 2−4 mm^2.

Results and Discussion

Figure 1 A−H is a set of extinction spectra demonstrating the broad wavelength tunability of the LSPR over the entire visible spectrum (viz. 400−800 nm). This has been accomplished by independently controlling the in-plane diameter, *a*, out-of-plane height, *b*, and in-plane shape of the constituent nanoparticles. The chemical composition of the nanoparticles, the substrate, and the surrounding dielectric medium are held constant. Figure 2 shows AFM images and line scans representative of the types of Ag nanoparticle arrays used in the optical extinction studies. Table 1 summarizes the Ag nanoparticle structural parameters and λ_{max} for the extinction spectra shown in Figure 1. Each spectrum has been scaled along the extinction axis by a factor (listed in Table 1) to normalize the data for presentation purposes. The oscillatory signal superimposed on the LSPR spectrum seen in the data is due to interference of the probe beam between the front and back faces of the mica substrate.[58]

The extreme sensitivity of λ_{max} to nanoparticle height can be illustrated by comparing the LSPR spectra in Figure 1 F−H. The nanoparticles that produce these spectra have identical shapes and values of the in-plane diameter, *a*, but vary in out-of-plane height, *b*, from 59 to 55 to 50 nm and result in a red shift of λ_{max} from 720 to 747 to 782 nm. This corresponds to a height sensitivity factor $\Delta\lambda_{max}/\Delta b = 7$. Figure 3 further illustrates the height sensitivity of the LSPR with a larger data set in the 500−600 nm region of the visible. Similar to Figures 1F−H, all the spectra in Figure 3 were generated from nanoparticle arrays prepared using the same size of diameter sphere mask; however, greater care was taken to vary the out-of-plane height over a larger range in order to provide a better estimate of LSPR peak shift versus change in height in this spectral region. Here, all the nanoparticle arrays were prepared using a 310 nm diameter sphere mask which is significantly smaller than the 542 nm mask used for Figures 1F−H. Figure 4 displays a plot of LSPR λ_{max} versus nanoparticle height for the spectra shown in Figure 3. The slope of this plot gives $\Delta\lambda_{max}/\Delta b = -2$. The results presented in Figures 3 and 4 suggest two things: (1) the LSPR spectra from nanoparticles with smaller in-plane widths are less sensitive to height changes, and (2) the LSPR height dependence is approximately linear over a height range of at least 25 nm. In a similar fashion, the in-plane width sensitivity factor $\Delta\lambda_{max}/\Delta a$ is illustrated by comparing Figures 1D, E, and H. These nanoparticles have identical shapes and approximately constant out-of-plane height but vary in in-plane diameter, *a*, from 90 to 120 to 145 nm. This change gives an estimate for $\Delta\lambda_{max}/\Delta a \approx 4$. Finally, the sensitivity of λ_{max} to nanoparticle shape changes is shown by comparing two pairs of LSPR spectra resulting from nanoparticles with approximately constant *a* and *b* but with in-plane shapes that are changed from triangular to ellipsoidal by postdeposition thermal annealing.

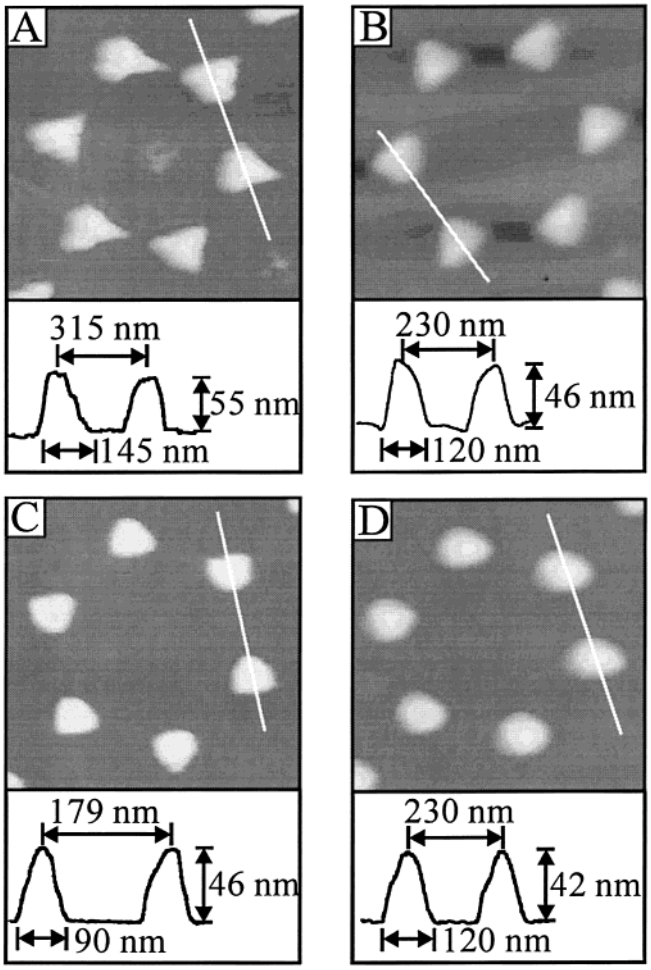

Figure 2. AFM images and line scans of representative Ag nanoparticle arrays on mica substrates. The line scan values reported here have not been deconvoluted for tip broadening effects. (A) 870 × 870 nm image, $D = 542$ nm, $d_m = 56$ nm, corresponds to Figure 1G. (B) 580 × 580 nm image, $D = 401$ nm, $d_m = 48$ nm, corresponds to Figure 1E. (C) 400 × 400 nm image, $D = 310$ nm, $d_m = 46$ nm, corresponds to Figure 1D. (D) 590 × 590 nm image, $D = 401$ nm, $d_m = 48$ nm, annealed, corresponds to Figure 1A.

TABLE 1: Ag Nanoparticle Structural Parameters Corresponding to the UV−Vis Extinction Measurements in Figure 1

	A[a]	B[a]	C[a]	D	E	F	G	H
a[b](nm)	120 ± 12	150 ± 15	150 ± 15	90 ± 6	120 ± 6	145 ± 6	145 ± 6	145 ± 6
b (nm)	42 ± 5	70 ± 8	62 ± 8	46 ± 3	46 ± 3	59 ± 4	55 ± 4	50 ± 4
D (nm)	401 ± 7	542 ± 7	542 ± 7	310 ± 9	401 ± 7	542 ± 7	542 ± 7	542 ± 7
d_m (nm)	48	70	62	46	48	60	55	50
substrate	mica	mica	mica	mica	mica	mica	mica	mica
in-plane shape[c]	E	E	E	T	T	T	T	T
λ_{max} (nm)	426	446	497	565	638	720	747	782
λ_{max} (cm^{-1})	23,474	22,422	20,121	17,699	15,674	13,889	13,387	12,788
Γ (cm^{-1})	3460	3883	3940	2788	2180	1826	2483	2063
Q	6.78	5.77	5.11	6.35	7.19	7.61	5.39	6.20
extinction scaling factor	3.7	2.5	2.7	1.6	1.0	1.9	1.3	0.7

[a] Annealed at 300 °C for 1 h. [b] Not corrected for AFM tip convolution. [c] E = elliptical, T = triangular.

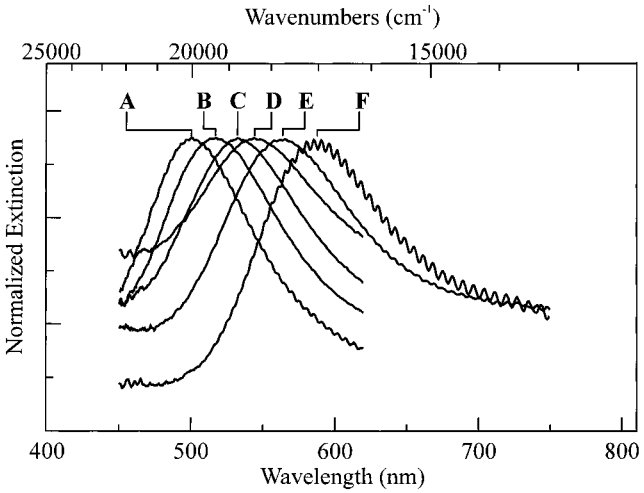

Figure 3. UV−vis extinction spectra for Ag nanoparticles arrays on glass. All spectra have a constant in-plane width produced from a nanosphere deposition mask with D = 310 nm (a = 90 ± 6 nm). Out-of-plane height, b, was varied. (A) b = 58 nm; λ_{max} = 501 nm. (B) b = 53 nm; λ_{max} = 517 nm. (C) b = 43 nm; λ_{max} = 533 nm. (D) b = 38 nm; λ_{max} = 544 nm. (E) b = 33 nm; λ_{max} = 563 nm. (F) b = 23 nm; λ_{max} = 585 nm.

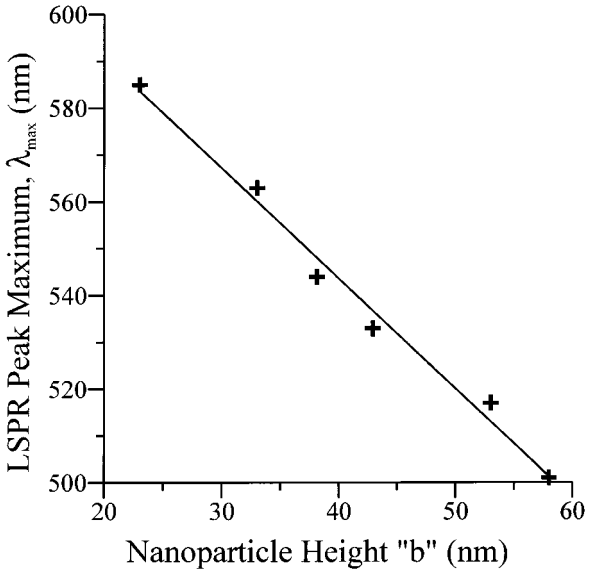

Figure 4. Plot of λ_{max} versus nanoparticle height, b, for the extinction spectra shown in Figure 3. The slope of the linear fit of the data indicates that a 1 nm change in nanoparticle height produces a 2 nm shift in LSPR peak maxima for nanoparticles with this in-plane width of approximately 90 nm.

Comparing Figures 1A and E, one finds a 212 nm blue shift in λ_{max} resulting from the thermal-annealing-induced shape change. A similar comparison of Figures 1C and F reveals a 223 nm blue shift. While these trends can be qualitatively understood by predictions of electrodynamic theory, the magnitude of the sensitivity of λ_{max} to nanoparticle structure has not been fully appreciated.[57,58] These results clearly show that the goal of nanoengineering the LSPR requires the use of high-precision nanofabrication techniques that provide size and shape control at the few nanometer level.

By increasing the size of the polystyrene nanosphere mask, D, it is possible to increase both the diameter and aspect ratio of the silver nanoparticles produced, thus shifting the LSPR frequency into the infrared region of the spectrum. Figure 5A,B represents the near-infrared LSPR spectra measured from two different arrays of particles on glass substrates, along with the corresponding AFM images and line scans. Table 2 lists the structural parameters of the Ag nanoparticles used to produce the spectra in Figure 5. In Figure 5B, we illustrate that we can engineer the nanoparticles to have their LSPR peak maxima in the approximate region of the optical communications wavelength of 1.5 μm. Mid-infrared LSPRs of Ag nanoparticles on silicon and germanium substrates were also measured using attenuated total reflection spectroscopy (ATR). The details of these measurements are given elsewhere.[41] The resulting spectra, corresponding AFM images, and line scans are shown in Figures

TABLE 2: Nanoparticle Structural Parameters Corresponding to the Near- and Mid-Infrared Extinction Measurements in Figures 5 and 6

	5A	5B	6A	6B
a[a](nm)	240 ± 15	323 ± 15	897 ± 72	830 ± 80
b (nm)	22 ± 2	28 ± 2	65 ± 3	50 ± 3
D (nm)	820 ± 15	1100 ± 15	2700 ± 70	2542 ± 80
d_m (nm)	20	25	65	50
substrate	glass	glass	silicon	germanium
in-plane shape[b]	T	T	T	T
λ_{max} (nm)	1125	1364	4739	6042
λ_{max} (cm^{-1})	8889	7331	2100	1655
Γ (cm^{-1})	1538	1914	1278	1361
Q	5.78	3.83	1.64	1.21

[a] Not corrected for AFM tip convolution. [b] T = triangular.

6A and 6B. These examples exhibited λ_{max} values at 2110 cm^{-1}, or 4739 nm and 1655 cm^{-1}, or 6042 nm, respectively. The nanoparticles in Figure 6A have a larger aspect ratio (16.6:1) than those in Figure 6B (13.8:1), and therefore exhibit a lower frequency LSPR. Also, the particles in Figure 6B were prepared on a germanium substrate, which has a higher dielectric constant than the silicon substrate used for 6A. This will also contribute to the red shifting of the LSPR in Figure 6B. In a separate study, these Ag nanoparticles were used for surface-enhanced infrared absorption (SEIRA) investigations.[41]

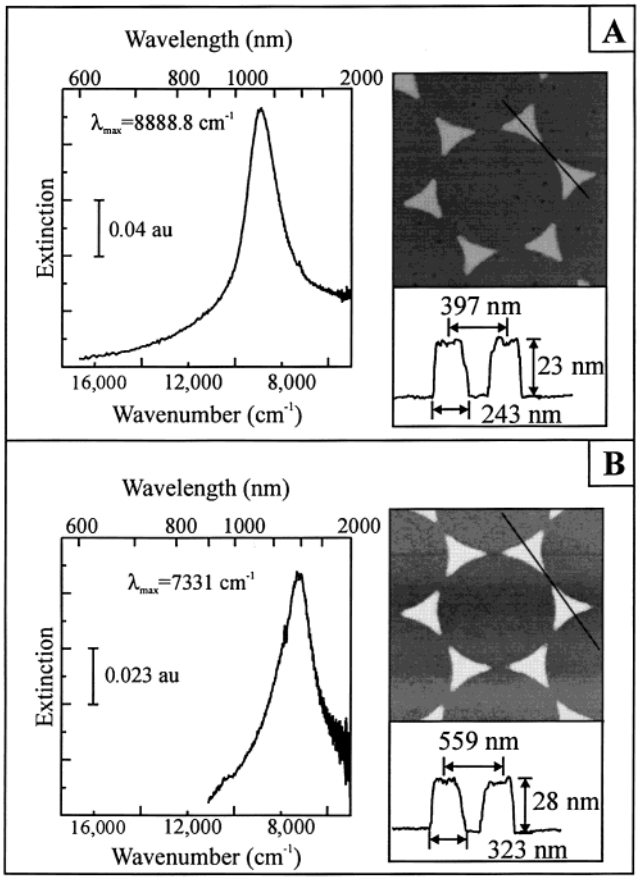

Figure 5. Near-IR extinction spectra, AFM images, and line scans of Ag nanoparticle arrays. See Table 2 for nanoparticle structural parameters.

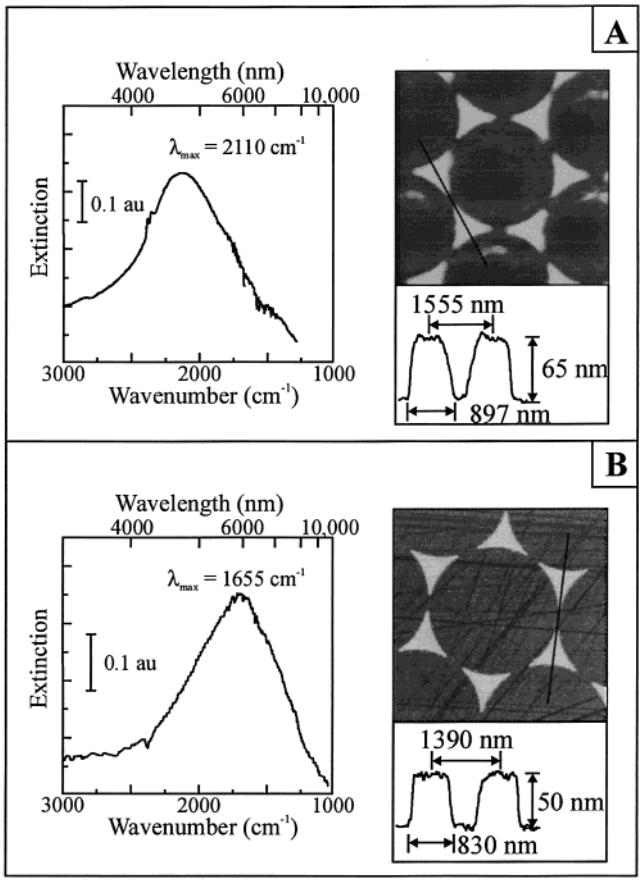

Figure 6. Mid-IR extinction spectra, AFM images, and line scans of Ag nanoparticle arrays. See Table 2 for nanoparticle structural parameters.

The spectra in Figures 1, 3, 5, and 6 establish the ability to tune throughout the visible and into the IR by changing either (1) the out-of-plane height, (2) the in-plane width, or (3) the shape of the individual nanoparticles. The data in Figures 7 and 8 demonstrate that broad spectral tunability can also be achieved by using dielectric overlayers of SiO_x. We have previously described how the optical properties of a Ag nanoparticle array depend on the external dielectric constant by measuring the LSPR in several solvents of varying refractive index.[59] In that study, it was shown that the LSPR systematically shifts to the red when the dielectric constant of the surrounding medium is increased. For all the spectra in Figures 1, 3, 5, and 6, the dielectric environment of the nanoparticles was kept constant and was comprised of a two-component system—the substrate and the surrounding ambient laboratory air. In Figure 7, the nanoparticles' dielectric environment becomes a more complex three-component system consisting of (1) the substrate, (2) the porous layer of SiO_x, and (3) the ambient air over the layer of SiO_x. Figure 7 shows that spectral manipulation throughout the visible region can be accomplished by using various thicknesses of SiO_x. Figures 7A−D illustrate that λ_{max} of the LSPR systematically shifts to the red when the SiO_x overlayer thickness is increased from 0 to 15 nm to 26 nm to 36 nm by making subsequent depositions. Figure 8 displays a plot of the SiO_x-induced LSPR peak shift, $\Delta\lambda_{max}$, versus the thickness of the SiO_x overlayer, d_{SiO_x}. The slope of the plot in Figure 8 gives the sensitivity factor $\Delta\lambda_{max}/\Delta d_{SiO_x} = 4$ over a thickness range of 36 nm. However, it is hypothesized that the shifting should curtail with increasing SiO_x thickness once "complete" encapsulation has occurred. Work is currently underway to investigate this hypothesis. Similarly, Figure 9A,B demonstrates that the same level of spectral manipulation can also be achieved in the near-IR region by using dielectric overlayers of SiO_x on larger nanoparticles. Again, both of the spectra in Figure 9, parts A and B, were generated from encapsulated nanoparticles which produced values of λ_{max} in the approximate region of 1.5 μm, the optical communications frequency. From the data presented in Figure 9, it is observed that SiO_x encapsulation narrows the Γ of the LSPR by approximately 3.5 times in cm^{-1} units. The

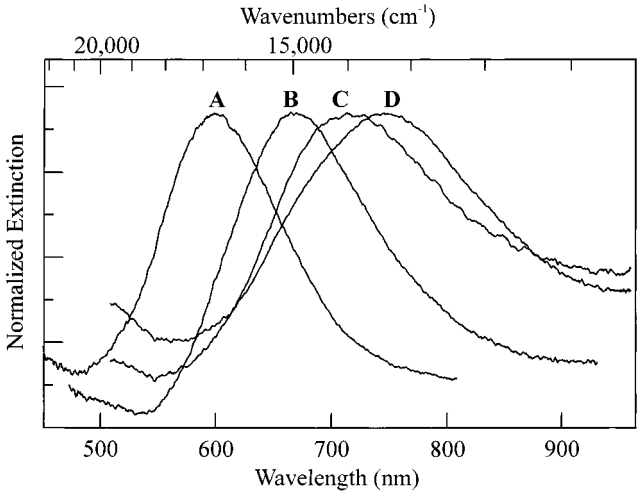

Figure 7. UV−vis extinction spectra for a Ag nanoparticle array (D = 400 nm, d_m = 25 nm) on glass with various thicknesses of SiO_x overlayers. (A) No SiO_x overlayer; λ_{max} = 597 nm. (B) SiO_x overlayer thickness = 15 nm; λ_{max} = 669 nm. (C) SiO_x overlayer thickness = 26 nm; λ_{max} = 714 nm. (D) SiO_x overlayer thickness = 36 nm; λ_{max} = 745 nm.

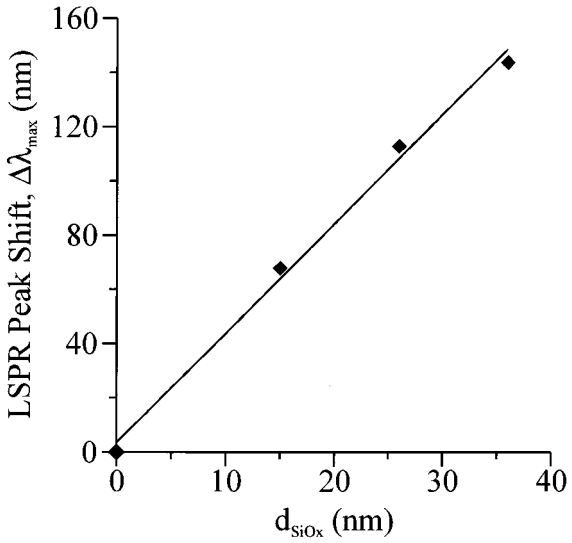

Figure 8. Plot of LSPR peak shift, $\Delta\lambda_{max}$, versus thickness of SiO_x overlayer. The slope of the linear fit of the data indicates that λ_{max} shifts to the red 4 nm for every 1 nm of SiO_x.

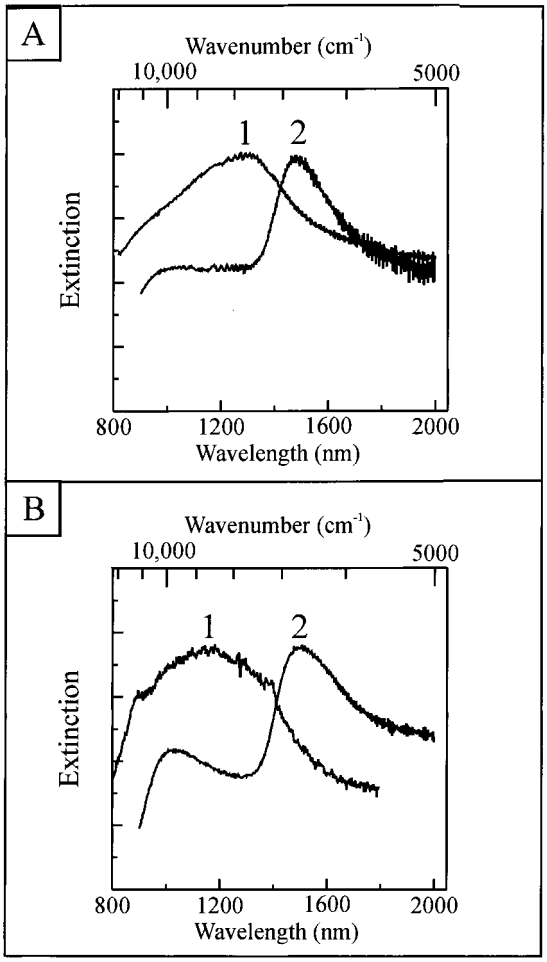

Figure 9. Near-IR extinction spectra for Ag nanoparticle arrays (D = 1100 nm, d_m = 50 nm) on glass with different thicknesses of SiO_x overlayers. (A-1) Extinction spectrum before SiO_x overlayer; λ_{max} = 1274 nm. (A-2) Extinction spectrum after deposition of 65 nm of SiO_x; λ_{max} = 1480 nm. (B-1) Extinction spectrum before SiO_x overlayer; λ_{max} = 1170 nm. (B-2) Extinction spectrum after deposition of 86 nm of SiO_x; λ_{max} = 1505 nm.

narrowing of this is not presently understood. Theoretical calculations are currently underway to investigate the effect of thin dielectric shells on the LSPR bandwidth of large, nonspherical Ag nanoparticles.

The results discussed above amply demonstrate the capability of NSL to fabricate nanoparticles with tunable LSPRs throughout the visible and into the infrared. However, broad spectral tunability is not the only important feature of the results presented here. It is also evident that the extinction spectra are quite intense when considering the number of nanoparticles sampled in the macroscopic probe beam. To assess the strength of the extinction, we have calculated the molar extinction coefficient and subsequently the oscillator strength. Optical extinction, E, for a transmission experiment is defined as

$$E = \log_{10}\frac{I_o}{I} = \frac{\sigma_E N_A}{2.303} \tag{1}$$

where I_o is the input light intensity, I is the transmitted light intensity, σ_E is the extinction cross section, and N_A is the areal density of the nanoparticle array. The magnitude of the optical extinction peak in Figure 1E is E = 0.11 at λ_{max} = 638 nm. The contribution of reflection losses from the exposed surfaces of the Ag nanoparticles was neglected in determining the total extinction value used to estimate the oscillator strength since it was expected to be small in comparison with the absorption and scattering contributions. The nanoparticle array has an areal density of $N_A = 1.52 \times 10^9$ nanoparticles cm^{-2} so that from eq 1 $\sigma_E = 1.66 \times 10^{-10}$ cm^2 $nanoparticle^{-1}$. The molar extinction coefficient is expressed as

$$\epsilon = \frac{\sigma_E M_{Ag}}{\rho_{Ag} V} \tag{2}$$

where M_{Ag} = 107.9 g mol^{-1}, ρ_{Ag} = 10.5 g cm^{-3}, and V is the volume of the nanoparticle = 1.57×10^{-16} cm^3. Thus ϵ_{max} = 1.09×10^4 M^{-1} cm^{-1}. Small corrections to this value should be made to account for the fact that only about 20% of the total surface area is covered by the nanoparticle array and that absorption accounts for about 65% of the total extinction.[58] An appropriately corrected value of the extinction coefficient is $\epsilon_{max, corr} = 3.5 \times 10^4$ M^{-1} cm^{-1}. This value represents the extinction coefficient calculated on the basis of moles of Ag atoms. To convert to a value based on the moles of Ag nanoparticles, we must multiply by the number of Ag atoms per nanoparticle (3.5×10^4 M^{-1} cm^{-1} $\times$ 9.19×10^6 atoms/nanoparticle). Thus, on the basis of moles of Ag nanoparticles, $\epsilon_{max, corr} = 3.2 \times 10^{11}$ M^{-1} cm^{-1}. The oscillator strength, f, of a transition is defined as the following:[60]

$$f = \frac{m_e c}{\pi e^2 N_o}\int \epsilon \, d\upsilon \tag{3}$$

where m_e is the electronic mass, e the electronic charge, and N_o the number of metal atoms absorbing light in a cubic cm, ϵ the frequency-dependent extinction coefficient, and υ the frequency. Assuming that the peak is a perfect Lorentzian,[61] this approximates to $f \cong 4.6 \times 10^{-9}\epsilon_{max}\Gamma$, where ϵ_{max} is the peak extinction coefficient in units of M^{-1} cm^{-1}, and Γ is the half intensity in units of cm^{-1}. The oscillator strength of the transition corresponding to the LSPR shown in Figure 1E is calculated to be 0.3 based on a Γ (fwhm) of 2180 cm^{-1}. In Table 3, we compare the values of the f, ϵ_{max}, and Γ of Ag atoms measured in both the gas and liquid phases to those calculated for the Ag nanoparticle array measured in Figure 1E. We find that the oscillator strength of our Ag nanoparticles is approximately the same as that of a Ag atom.

TABLE 3: Peak Extinction Coefficients (ϵ_{max}), Half-intensity Bandwidths (Γ), and Oscillator Strengths (f), of Silver in Various Systems

system	ϵ_{max} (M^{-1} cm^{-1})	Γ (cm^{-1})	f
Ag atom (gas phase)	9.8×10^{8} [a]	0.10	0.46
Ag atom (aqueous)	1.6×10^{4} [b]	7340	0.54
Ag nanoparticle (ambient)	3×10^{4} [c]	2223	0.3

[a] See refs 70,71. [b] See ref 72. [c] This work.

We have discussed in detail the dependence of λ_{max} on Ag nanoparticle structure as well as the large oscillator strength of these localized surface plasmon resonances. We now turn to a discussion of the LSPR bandwidth. In all of the LSPR spectra reported here, the bandwidths are sufficiently narrow that they are likely to be determined by intrinsic electron relaxation dynamics rather than size inhomogeneity. Indeed, the observed bandwidths in the visible range between 1826 $cm^{-1} < \Gamma < 3940$ cm^{-1} and are consistent with recent measurements of femtosecond relaxation dynamics in metallic nanoparticles.[62] To the best of our knowledge, the narrowest LSPR bandwidth reported is 1000 cm^{-1} for ~40 nm diameter Au nanoparticles embedded in a high external dielectric constant medium (TiO_2).[63] If the nanoparticles corresponding to our narrowest LSPR had been embedded in TiO_2, we estimate, based on Mie theory model calculations of spherical Ag/TiO_2 core−shell nanoparticles, that the G would have been reduced by a factor of ~2. To further set our results in context, the "sharpness" of our LSPR spectra as reflected by the quality factor, $Q = \lambda_{max}/\Gamma$, are reported in Tables 1 and 2. For LSPRs in the visible and near-infrared, we find that $3.83 < Q < 7.61$. We conclude that the wavelength-tunable resonances observed for our NSL-fabricated Ag nanoparticles are significantly sharper than those reported for wavelength-tunable Au nanoshells which show $Q < 2$.[52,53]

Conclusions

In conclusion, nanosphere lithography, NSL, was used to fabricate Ag nanoparticles that displayed localized surface plasmon resonances, LSPRs, tunable throughout the visible, near-infrared, and mid-infrared regions of the electromagnetic spectrum. We accomplished this unprecedented level of wavelength agility by independently varying the nanoparticle height, width, shape, and dielectric environment. We presented and discussed five new features of Ag nanoparticle optics: (1) the peak extinction wavelength, λ_{max}, shifts 2−5 nm per 1 nm variation in nanoparticle width and height; (2) changing the in-plane nanoparticle shape from triangular to ellipsoidal shifts λ_{max} ~200 nm; (3) broad wavelength tunability was achieved while preserving narrow LSPR line widths, Γ; (4) the LSPR of Ag nanoparticles encapsulated in thin overlayers of SiO_x red shift 4 nm for every 1 nm of SiO_x thickness; and (5) the oscillator strength of our Ag nanoparticles is 0.3 which is comparable to that of a Ag atom in the gas or liquid phase. Work is in progress to utilize discrete dipole approximation methods[58,64,65] to accurately model and further understand the size dependence of these extinction spectra.

The ability to produce nanoparticle arrays with wavelength-tunable LSPRs opens up new applications in both linear and nonlinear spectroscopy. NSL-fabricated nanoparticles may provide unprecedented levels of sensitivity in surface-enhanced Raman and related spectroscopies. By tuning the excitation laser to the surface plasmon resonance, it should be possible to maximize the local electromagnetic field enhancement. We are currently exploring the nonlinear optical properties of these nanoparticles, opening up new applications for optical limiting, sensitive infrared detection,[66,67] and light modulation. We anticipate that the surface-enhancing properties of size-tunable nanoparticles will be exploited for chemosensor and biosensor applications.[68,69]

Acknowledgment. Funding was provided by the ARO (Grant DAAG55-97-1-0133), NSF (Grant CHE-940078), and the MRSEC program of the NSF (Grant DMR-9632472). The authors also acknowledge George C. Schatz and Mark A. Ratner for helpful discussions about this work. Also, we thank Joseph T. Hupp and Robert Johnson for providing access to the OLIS-modified Cary 14 spectrophotometer used to measure near-IR extinction spectra.

References and Notes

(1) Kreibig, U.; Vollmer, M. *Optical Properties of Metal Clusters*; Springer-Verlag: Heidelberg, Germany, 1995; Vol. 25.
(2) Quinten, M.; Leitner, A.; Krenn, J. R.; Aussenegg, F. R. *Opt. Lett.* **1998**, *23*, 1331−1333.
(3) Krenn, J. R.; Dereux, A.; Weeber, J. C.; Bourillot, E.; Lacroute, Y.; Goudonnet, J. P. *Phys. Rev. Lett.* **1999**, *82*, 2590−2593.
(4) Novotny, L.; Bian, R. X.; Xie, S. *Phys. Rev. Lett.* **1997**, *79*, 645−648.
(5) Jersch, J.; Dickmann, K. *Appl. Phys. Lett.* **1996**, *68*, 868−870.
(6) Jersch, J.; Demming, F.; Dickmann, K. *Appl. Phys. A* **1997**, *64*, 29−32.
(7) Jersch, J.; Demming, F.; Hildenhagen, L. J.; Dickmann, K. *Appl. Phys. A* **1998**, *66*, 29−34.
(8) Ebbesen, T. W.; Lezec, H. J.; Ghaemi, H. F.; Thio, T.; Wolff, P. A. *Nature* **1998**, *391*, 667−669.
(9) Pendry, J. B. *Science* **1999**, *285*, 1687−1688.
(10) Pufall, M. R.; Berger, A.; Schultz, S. *J. Appl. Phys.* **1997**, *81*, 5689−5691.
(11) Hamann, H. F.; Gallagher, A.; Nesbitt, D. J. *Appl. Phys. Lett.* **1998**, *73*, 1469−1471.
(12) Knoll, B.; Kellmann, F. *Nature* **1999**, *399*, 134−137.
(13) Sánchez, E. J.; Novotny, L.; Xie, X. S. *Phys. Rev. Lett.* **1999**, *82*, 4014−4017.
(14) Gu, M.; Ke, P. C. *Opt. Lett.* **1999**, *24*, 74−76.
(15) Svoboda, K.; Block, S. M. *Opt. Lett.* **1994**, *19*, 930−932.
(16) Feldstein, M. J.; Keating, C. D.; Liau, Y.-H.; Natan, M. J.; Scherer, N. F. *J. Am. Chem. Soc.* **1997**, *119*, 6638−6647.
(17) Fukumi, K.; Chayahara, A.; Kadono, K.; Sakaguchi, T.; Horino, Y.; Miya, M.; Fujii, K.; Hayakawa, J.; Satou, M. *J. Appl. Phys.* **1994**, *75*, 3075−3079.
(18) Haglund, R. F., Jr.; Yang, L.; Magruder, R. H., III; Wittig, J. E.; Becker, K.; Zuhr, R. A. *Opt. Lett.* **1993**, *18*, 373−375.
(19) Neuendorf, R.; Quinten, M.; Kreibig, U. *J. Chem. Phys.* **1996**, *104*, 6348−6354.
(20) Haus, J. W.; Kalyaniwalla, N.; Inguva, R.; Bowden, C. M. *J. Appl. Phys.* **1989**, *65*, 1420−1423.
(21) Elghanian, R.; Storhoff, J. J.; Mucic, R. C.; Letsinger, R. L.; Mirkin, C. A. *Science* **1997**, *277*, 1078−1081.
(22) Bauer, G.; Pittner, F.; Schalkhammer, T. *Mikrochim. Acta* **1999**, *131*, 107−114.
(23) Dirix, Y.; Bastiaansen, C.; Caseri, W.; Smith, P. *Adv. Mater.* **1999**, *11*, 223−227.
(24) Kroschwitz, J. I.; Howe-Grant, M. Glass. In *Encyclopedia of Chemical Technology*, 4th ed.; Kroschwitz, J. I., Howe-Grant, M., Eds.; John Wiley & Sons: New York, 1994; Vol. 12, pp 569−571.
(25) Campion, A.; Kambhampati, P. *Chem. Soc. Rev.* **1998**, *27*, 241−250.
(26) Nie, S.; Emory, S. R. *Science* **1997**, *275*, 1102−1106.
(27) Emory, S. R.; Nie, S. *Anal. Chem.* **1997**, *69*, 2631−2635.
(28) Emory, S. R.; Nie, S. *J. Phys. Chem. B* **1998**, *102*, 493−497.
(29) Emory, S. R.; Haskins, W. E.; Nie, S. *J. Am. Chem. Soc.* **1998**, *120*, 8009−8010.
(30) Emory, S. R.; Nie, S. *Nature* **1998**.
(31) Michaels, A. M.; Nirmal, M.; Brus, L. E. *J. Am. Chem. Soc.* **1999**, *121*, 9932−9939.
(32) Kneipp, K.; Kneipp, H.; Deinum, G.; Itzkan, I.; Dasari, R. R.; Feld, M. S. *Appl. Spectrosc.* **1998**, *52*, 175−178.
(33) Kneipp, K.; Kneipp, H.; Kartha, V. B.; Manoharan, R.; Deinum, G.; Itzkan, I.; Dasari, R. R.; Feld, M. S. *Phys. Rev. E* **1998**, *57*, R6281−R6284.
(34) Kneipp, K.; Wang, Y.; Kneipp, H.; Perelman, L. T.; Itzkan, I.; Dasari, R. R.; Feld, M. S. *Phys. Rev. Lett.* **1997**, *78*, 1667−1670.
(35) Van Duyne, R. P.; Hulteen, J. C.; Treichel, D. A. *J. Chem. Phys.* **1993**, *99*, 2101−2115.

(36) Caldwell, W. B.; Chen, K.; Herr, B. R.; Mirkin, C. A.; Hulteen, J. C.; Van Duyne, R. P. *Langmuir* **1994**, *10*, 4109−4115.
(37) Yang, W. H.; Hulteen, J. C.; Schatz, G. C.; Van Duyne, R. P. *J. Chem. Phys.* **1996**, *104*, 4313−4323.
(38) Pipino, A. C. R.; Schatz, G. C.; Van Duyne, R. P. *Phys. Rev. B* **1996**, *53*, 4162−4169.
(39) Wadayama, T.; Suzuki, O.; Takeuchi, K.; Seki, H.; Tanabe, T.; Suzuki, Y.; Hatta, A. *Appl. Phys. A* **1999**, *69*, 77−80.
(40) Tarcha, P. J.; DeSaja-Gonzalez, J.; Rodriguez-Llorente, S.; Aroca, R. *Appl. Spectrosc.* **1999**, *53*, 43−48.
(41) Jensen, T. R.; Van Duyne, R. P.; Johnson, S. A.; Maroni, V. A. *Appl. Spectrosc.* **2000**, *54*, 371−377.
(42) Jeanmaire, D. L.; Van Duyne, R. P. *J. Electroanal. Chem.* **1977**, *84*, 1−20.
(43) Xu, H.; Bjerneld, E. J.; Käll, M.; Börjesson, L. *Phys. Rev. Lett.* **1999**, *83*, 4357−4360.
(44) Craighead, H. G.; Niklasson, G. A. *Appl. Phys. Lett.* **1984**, *44*, 1134−1136.
(45) Acker, W. P.; Schlicht, B.; Chang, R. K.; Barber, P. W. *Opt. Lett.* **1987**, *12*, 465.
(46) Gotschy, W.; Vonmetz, K.; Leitner, A.; Aussenegg, F. R. *Appl. Phys. B* **1996**, *63*, 381−384.
(47) Gotschy, W.; Vonmetz, K.; Leitner, A.; Aussenegg, F. R. *Opt. Lett.* **1996**, *21*, 1099−1101.
(48) Hornyak, G. L.; Patrissi, C. J.; Martin, C. R. *J. Phys. Chem. B* **1997**, *101*, 1548−1555.
(49) Hornyak, G. L.; Martin, C. R. *Thin Solid Films* **1997**, *303*, 84−88.
(50) Al-Rawashdeh, N. A. F.; Sandrock, M. L.; Seugling, C. J.; Foss, C. A., Jr. *J. Phys. Chem. B* **1998**, *102*, 361−371.
(51) Buncick, M. C.; Warmack, R. J.; Ferrell, T. L. *J. Opt. Soc. Am. B* **1987**, *4*, 927−933.
(52) Oldenburg, S. J.; Jackson, J. B.; Westcott, S. L.; Halas, N. J. *Appl. Phys. Lett.* **1999**, *75*, 2897−2899.
(53) Oldenburg, S. J.; Averitt, R. D.; Westcott, S. L.; Halas, N. J. *Chem. Phys. Lett.* **1998**, *288*, 243−247.
(54) Westcott, S. L.; Oldenburg, S. J.; Lee, T. R.; Halas, N. J. *Langmuir* **1998**, *14*, 5396−5401.
(55) Hulteen, J. C.; Treichel, D. A.; Smith, M. T.; Duval, M. L.; Jensen, T. R.; Van Duyne, R. P. *J. Phys. Chem. B* **1999**, 3854−3863.
(56) Hulteen, J. C.; Van Duyne, R. P. *J. Vac. Sci. Technol. A* **1995**, *13*, 1553−1558.
(57) Zeman, E. J.; Schatz, G. C. *J. Phys. Chem.* **1987**, *91*, 634−643.
(58) Jensen, T. R.; Schatz, G. C.; Van Duyne, R. P. *J. Phys. Chem. B* **1999**, 2394−2401.
(59) Jensen, T. R.; Duval, M. L.; Kelly, L.; Lazarides, A.; Schatz, G. C.; Van Duyne, R. P. *J. Phys. Chem. B* **1999**, 9846−9853.
(60) Willard, H. H.; Merritt, L. L., Jr.; Dean, J. A. *Instrumental Methods of Analysis*, Fourth ed.; D. Van Nostrand Company, Inc.: Princeton, NJ, 1965.
(61) Drago, R. S. *Physical Methods for Chemists*, 2nd ed.; Saunders College Publishing: Harcourt Brace Jovanovich College Publishers, Fort Worth, TX, 1992.
(62) Link, S.; El-Sayed, M. A. *J. Phys. Chem. B* **1999**, *103*, 8410−8426.
(63) Klar, T.; Perner, M.; Grosse, S.; von Plessen, G.; Spirkl, W.; Feldmann, J. *Phys. Rev. Lett.* **1998**, *80*, 4249−4252.
(64) Yang, W. H.; Schatz, G. C.; Van Duyne, R. P. *J. Chem. Phys.* **1995**, *103*, 869−875.
(65) Jensen, T. R.; Kelly, L.; Lazarides, A.; Schatz, G. C. *J. Clust. Sci.* **1999**, *10*, 295−317.
(66) Stuart, H. R.; Hall, D. G. *Appl. Phys. Lett.* **1998**, *73*, 3815−3817.
(67) Stuart, H. R.; Hall, D. G. *Appl. Phys. Lett.* **1996**, *69*, 2327−2329.
(68) Malinsky, M. D.; Jensen, T. R.; Van Duyne, R. P. Submitted.
(69) Kreibig, U.; Gartz, M.; Hilger, A. *Ber. Bunsen-Ges. Phys. Chem.* **1997**, *101*, 1593−1604.
(70) Wiese, W. L.; Smith, M. W.; Glennon, B. M. *Atomic Transition Probabilities*; National Bureau of Standards: Washington, DC, 1966; Vol. I.
(71) Wiese, W. L.; Smith, M. W.; Glennon, B. M. *Atomic Transition Probabilities*; National Bureau of Standards: Washington, DC, 1969; Vol. II.
(72) Ershov, B. G.; Janata, E.; Henglein, A.; Fojtik, A. *J. Phys. Chem.* **1993**, *97*, 4589−4594.